Role of structural defects on the half-metallic character of Co_2MnGe and Co_2MnSi Heusler alloys

S. Picozzi and A. Continenza
INFM - Dipartimento di Fisica, Università L'Aquila, 67010 Coppito, L'Aquila, Italy

A. J. Freeman
Department of Physics and Astronomy, Northwestern University, 60208 Evanston, Illinois, USA
(Received 23 October 2003; published 22 March 2004)

Heusler alloys, such as Co_2MnSi and Co_2MnGe, have been predicted from first–principles to be half metallic and potential candidates for spintronic applications. However, spin polarizations of only 50–60 % were experimentally obtained for these compounds—a decrease attributed to defects in the Mn and Co sublattices. Accurate *ab initio* full-potential linearized augmented plane wave calculations are performed in order to determine the effects of several types of defects (such as antisites and atomic swaps) on the electronic and magnetic properties of the bulk Heusler compounds. Our findings, in general agreement with experiments, show that Mn antisites have the lowest formation energy and retain the half-metallic character. On the other hand, Co antisites have a slightly higher formation energy and a dramatic effect on the electronic properties: the defect states that locally destroy half metallicity are energetically localized and are screened out in a couple of atomic shells. In this case, the spin polarization at the Fermi level is strongly reduced, and the spin polarization due to the *s* electrons, responsible for the tunneling current, is in excellent agreement with experiment. Finally, both Mn-Si and Mn-Co atomic swaps have very high formation energies, keeping however the half-metallic character.

DOI: 10.1103/PhysRevB.69.094423 PACS number(s): 75.50.Cc, 71.55.−i

I. INTRODUCTION

One of the key properties in magneto electronics is the so-called half metallicity, i.e., conduction electrons that are 100% spin polarized—due to a gap at the Fermi level, E_F, in the minority-spin channel—and a finite density of states at E_F for the majority spin channel. Heusler alloys—and in particular Co_2MnGe and Co_2MnSi—were predicted from first principles[1,2] to be half metallic, along with a remarkably high Curie temperature. Therefore, in principle, they are ideal materials for spintronic applications, such as tunneling magnetoresistance (TMR) and giant magnetoresistance (GMR) elements; however, polarizations of the order of only 50–60 %[3–5] have so far been measured, thus hindering their practical use. Ambrose *et al.*[6] deposited Co_2MnGe films on a GaAs substrate by molecular-beam epitaxy; their measurements revealed the perfect crystallinity of the Heusler films up to a 350 Å thickness and a large magnetization along with a small magnetic anisotropy. The magnetic, structural, and transport properties of Co_2MnSi were reported for sputtered thin films and a single crystal.[5] Neutron diffraction showed the disorder to be zero for Mn-Si antisite, but extensive for Co-Mn disorder; in particular, as much as 14% of Mn sites are occupied by Co and 5–7% of Co sites are occupied by Mn atoms. Similar results were obtained from EXAFS and neutron diffraction for Co_2MnSi large grain or powder samples.[7] Atomic disorder in Co_2MnGe was measured by anomalous x-ray diffraction: about 12.7% of the Mn sublattice were occupied by Co, consistent with the observed deviation from stoichiometry.

From the theoretical point of view, pioneering Korringa-Kohn–Rostoker (KKR) calculations performed for Co_2MnGe and Co_2MnSi bulk compounds predicted for the first time half metallicity in these compounds.[1] More recently, calculations performed by the same authors for Co_2MnSi and Co_2MnGe surfaces[8] showed that the half-metallic character was strongly dependent on the type (i.e., Co_2MnSi films are generally half metallic, Co_2MnGe films are not), surface termination (Mn and Si-terminated [001] surfaces are generally half metallic, Co-terminated ones are not), growth direction, and thickness of the film. Within this same framework, density-functional layer KKR simulations within the coherent potential approximation by Orgassa *et al.*[9] for the half-Heusler compound NiMnSb showed that atomic disorder (i.e., interchange of Ni and Mn or vacancies) at the level experimentally observed in thin films leads to minority-spin states at E_F, resulting in the loss of the half-metallic character.

Since atomic disorder was suggested as a mechanism to reduce spin polarization, we investigated in a previous paper[10] the Co antisite defect in Co_2MnGe and found that half metallicity could be lost due to defect-induced minority gap states. However, these states are efficiently screened out, as shown by the fast decay of the minority-spin charge density around E_F as a function of the distance from the defective site. In the present work, we extend our analysis by systematically investigating the effects of several kind of defects (such as swaps and antisites) in both Co_2MnSi and Co_2MnGe hosts, in terms of formation energy and defect-induced electronic and magnetic properties. In particular, according to experiments, the most likely defects are: (i) Mn antisites where a Co atom is replaced by a Mn, (ii) Co antisites where a Mn atom is replaced by a Co, (iii) Co-Mn swaps, where a Mn-Co nearest-neighbor pair shows ex-

changed positions compared to the ideal bulk, and (iv) Mn-Si swaps in Co_2MnSi, where a Mn-Si second-nearest-neighbor pair shows exchanged positions compared to the bulk. Mn–Ge swaps in Co_2MnGe have not been considered, since no experiments have ever suggested this kind of disorder and our calculations suggest in Co_2MnSi that this kind of swaps is extremely unfavorable (see below). Recall that for antisites (swaps) the bulk stoichiometry is not preserved (preserved), since, for example, the Co antisite in Co_2MnSi leads to a $Co_2Co_xMn_{1-x}Si$ compound.

The work is organized as follows: in Sec. II we report structural and computational details, in Sec. III we discuss results for the different defects considered and different hosts and in Sec. IV we summarize our conclusions.

II. TECHNICAL AND STRUCTURAL DETAILS

The calculations were performed using a 32 atom unit cell, obtained by considering the $L2_1$ bulk unit cell (with four atoms) and doubling its Bravais vectors (i.e., the defective cell is $2\times2\times2$ times the $L2_1$ unit cell). In order to check the convergence of the results as a function of the unit-cell dimensions, we performed some test calculations using 64 atoms; we obtained only small quantitative changes in the relevant properties, but, qualitatively, the physical results are the same as those obtained for the smaller 32-atoms cell. The lattice constant was kept fixed to the calculated bulk equilibrium value[2]—within the generalized gradient approximation (GGA) (Ref. 11), i.e., $a(Co_2MnGe)=10.84$ a.u. and $a(Co_2MnSi)=10.65$ a.u.; it was previously shown that GGA reproduces the correct experimental values [$a^{expt}(Co_2MnGe)=10.85$ a.u. and $a^{expt}(Co_2MnSi)=10.68$ a.u.], in contrast with the local spin-density approximation (LSDA) which predicts a 10% volume underestimation.[2] Internal degrees of freedom were fully relaxed according to *ab initio* atomic forces.

The simulations were performed within the GGA (Ref. 11) to density-functional theory, using the all-electron full-potential linearized augmented plane wave (FLAPW) (Ref. 12) method. Muffin-tin (MT) radii were set to $R_{\mathrm{MT}}=2.1$ a.u.; in the interstitial part, a wave function cutoff $k_{max}=3.8$ a.u.$^{-1}$ was used. The Brillouin zone was sampled using up to 20 special **k** points.[13]

The formation energy is estimated as[14]

$$\Delta E = E^{def} - E^{id} + n_{\mathrm{Mn}}\mu^0_{\mathrm{Mn}} + n_{\mathrm{Co}}\mu^0_{\mathrm{Co}} + n_X\mu^0_X, \qquad (1)$$

where E^{def} and E^{id} are the total energies of the unit cell with and without defect, respectively; n_i takes into account that, in forming the defect, n_i atoms are transferred to or from a chemical reservoir that has a characteristic energy μ^0_i. In our case, we choose as the stable phase for element i [$i=$Mn, Co, X (= Si, Ge)], the [001]-ordered fcc antiferromagnetic Mn (Ref. 15), the ferromagnetic hcp Co (Ref. 15), and the Si (or Ge) diamondlike structure, respectively. Charged defects or competing crystalline phases that might be formed during defective growth are not taken into account.

TABLE I. Formation energy (in eV) and total magnetic moments (in Bohr magnetons) for the different defects in Co_2MnGe and Co_2MnSi hosts.

	Co_2MnSi		Co_2MnGe	
	ΔE	M_{tot}	ΔE	M_{tot}
Co antisite	0.80	38.01	0.84	38.37
Mn antisite	0.33	38.00	0.33	38.00
Co-Mn swap	1.13	36.00	1.17	36.00
Mn-Si swap	1.38	40.00		

Moreover, the equilibrium concentration of the defect at temperature T, considering a Boltzmann–like distribution, can be estimated as[16]

$$D_{def} = N_{sites}\exp\left(-\frac{\Delta E}{k_B T}\right), \qquad (2)$$

where N_{sites} is the number of available sites.

III. RESULTS AND DISCUSSION

In Table I, we report the calculated formation energies for all the defects considered in the two different matrices; we also show the total magnetic moment in the unit cell. Recall that both Co_2MnGe and Co_2MnSi in their bulk phase show a total magnetic moment of 5 μ_B (or, equivalently, a magnetic moment of 40 μ_B in the 32-atoms unit cell used for the defect calculations).[2]

A. Mn antisite defect in Co_2MnSi

The considerably small value obtained ($\Delta E=0.33$ eV) suggests that this kind of defect is likely to be formed during Co_2MnSi growth. In particular, considering a temperature $T=1523$ K, suitable for a triarc Czochralski growth of bulk Co_2MnSi,[5] the Mn antisite concentration can reach the high value of 0.36×10^{22} cm^{-3}, corresponding to about 8%. This is in good agreement with the reported experimental value of 5–7 %.[5] However, we would like to point out that ours is only a rough quantitative estimate, since Eq. (2) is strictly valid in the limit of very low concentrations that are highly exceeded when considering more than a few percent.

Let us now discuss the electronic and magnetic properties of the system, focussing in particular on the defect-induced changes on half metallicity. In Fig. 1 we show the total density of states (DOS) of both the defective and the ideal systems. The comparison shows that the defect induces only minor modifications—such as features at -1.5 eV and -0.8 eV for the majority-spin states; on the other hand, due to the Mn antisite, a rigid shift of about 0.05 eV towards higher binding energies occur in the minority-spin channel. This results in a very small increase of the spin gap (0.34 eV and 0.39 eV in the ideal and defective systems, respectively). However, it is clear that half metallicity is kept even in the presence of the antisite, the total magnetic moment being $38\mu_B$ and $40\mu_B$ in the defective and ideal unit cells, respectively. We remark that, interestingly, the half-metallic char-

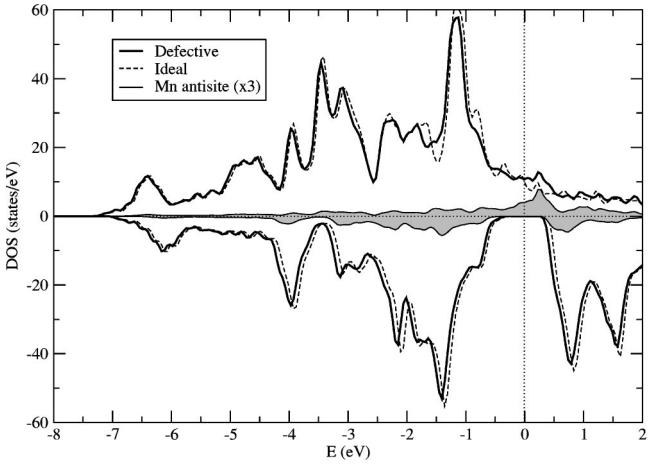

FIG. 1. Total DOS for defective (solid bold line) and ideal (dashed line) Co_2MnSi with Mn antisite in Co_2MnSi; majority spin shown positive and minority spin negative. The Mn-antisite PDOS (multiplied by a factor of 3) is also shown (gray shaded area).

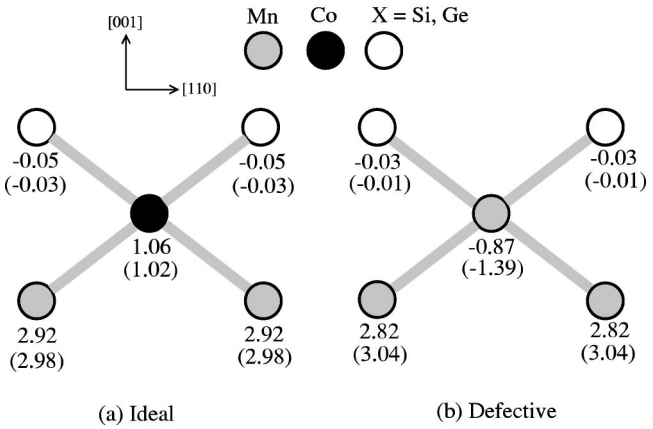

FIG. 2. Magnetic moments within MT spheres for (a) ideal and (b) defective systems for the Mn antisite in Co_2MnSi around the defect. Values in parenthesis denote magnetic moments for equivalent atoms in Co_2MnGe.

acter is kept thanks to a charge balance granted by the majority component only. In fact, in this case, the total charge differs from the ideal case by $\Delta Z=-2$ electrons; since the number of occupied states in the minority channel does not change (see Fig. 1, $\Delta N_{-}=0$), then the variation of occupied states in the majority component must account for the total ΔZ (i.e., $\Delta N_{+}=-2$ electrons). In particular, the two-electron states appear as a new peak at ~ 0.3 eV above E_F, almost entirely due to the Mn-antisite *d* states, as shown by the corresponding feature in the DOS projected (PDOS) on the Mn defective site (see shaded area in Fig. 1). Our results are particularly relevant in the spin-injection framework: even if the Mn antisite defects—due their low formation energies - are most likely to occur during Co_2MnSi growth, the most important property of this Heusler alloy, i.e., its half metallicity, is kept. Therefore, experimental results reporting a polarization lower than the expected 100% needs to be explained invoking surface effects[8] or other types of bulk defects (such as Co antisites[4,3]—see below—, vacancies, interstitials, etc.).

Further insights can be gained from the magnetic moments of the different atomic species. In Fig. 2, we report a schematic view of the region close to the defect (i.e., the Mn antisite and its first nearest neighbors along the [110] direction) as compared with the same region in the ideal Heusler alloy, including the relative magnetic moments in the MT spheres. Here and in the following similar figures, we report only these few atoms since (i) other symmetry directions (i.e., $[1\bar{1}0]$) show an equivalent behavior and (ii) farther atomic shells do not show variations of their magnetic moments larger than 1%—with respect to their bulk values—and/or are below our numerical precision ($0.01\mu_B$). The central Mn antisite accounts for all the defect-induced reduction of $2\mu_B$ in the total magnetic moment, since it has a magnetic moment of $-0.87\mu_B$ and substitutes for a Co having a magnetic moment of $1.06\mu_B$. The large change in the atomic magnetization (which also reverses its sign) on the defect site shows that a large rearrangement of the charge and spin densities occur when the defect is introduced, as shown by the completely different projected DOS (not reported) on the Mn defect site compared to Mn in bulk Co_2MnSi. Only small changes are observed on its nearest neighbors. This shows that the defect-induced effects are efficiently screened out in the Co_2MnSi matrix; incidentally, these findings support our computational choice of a relatively small unit cell.

B. Co antisite defect in Co_2MnSi

A slightly higher formation energy is calculated for the Co antisite. This increase, however results, according to Eq. (2), in a concentration which is almost 2 order of magnitude smaller than that obtained for the Mn antisite. Therefore, although present, these defects are expected to have a relatively small density. This is actually at variance with experiments, which found Co and Mn antisites occurring with more or less the same concentrations. We think that, as pointed out, some errors may arise from the quantitative estimate of the concentrations for high defect density: Eq. (2) shows that small uncertainties in ΔE (due to the finite size of the unit cell, **k**-point sampling or other computational details) result in large errors in the defect concentration.

The analysis of the total DOS (see Fig. 3) shows a defect-induced dramatic change in the conducting character: half metallicity is lost, due to a very sharp peak located just in proximity to E_F. As shown in Fig. 3, there is an almost exact superposition between the ideal and defective total DOS, except for the peak at E_F. The projected density of states (not shown) reveals that this is almost entirely due to the antisite Co *d* states. In particular, this states accommodates two electrons (see below) and is double degenerate at the Brillouin-zone center with e_g symmetry. At variance with the Mn antisite defect, the total charge difference is $\Delta Z=+2$ electrons; being the majority DOS component almost unaffected with respect to the ideal case (see Fig. 3), the total charge variation is taken over by the peak in the DOS just

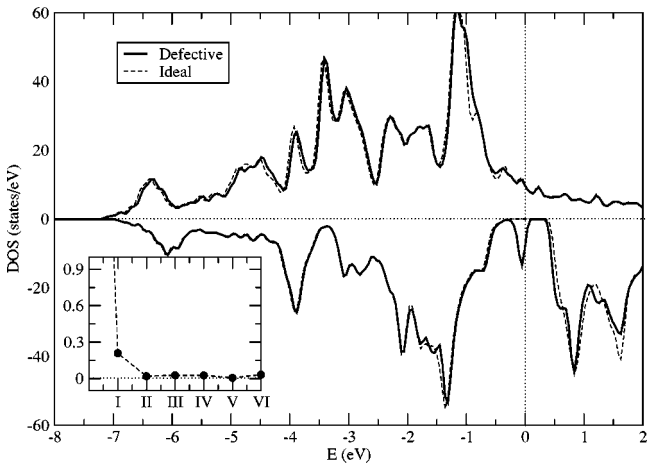

FIG. 3. Total DOS for defective (solid bold line) and ideal (dashed line) Co_2MnSi with Co antisite in Co_2MnSi. The inset shows the minority DOS at E_F projected on the different neighbors (denoted as roman numbers) as one moves away from the Co-antisite defect.

below E_F in the minority component only ($\Delta N_- = +2$ electrons). In this case, the spin polarization at the Fermi level, defined as:

$$P = \frac{N^{\uparrow}(E_F) - N^{\downarrow}(E_F)}{N^{\uparrow}(E_F) + N^{\downarrow}(E_F)}, \tag{3}$$

where $N^{\uparrow}(E_F)$ and $N^{\downarrow}(E_F)$, respectively, denote the up- and down-spin component of the total DOS at E_F, is as low as 6%. Moreover, since the tunneling current in experiments is dominated by the *s* electrons, we also calculated the *s* component of the spin polarization at E_F, defined as:

$$P_s = \frac{N_s^{\uparrow}(E_F) - N_s^{\downarrow}(E_F)}{N_s^{\uparrow}(E_F) + N_s^{\downarrow}(E_F)}. \tag{4}$$

Our result is $P_s = 55\%$, in (surprising) excellent quantitative agreement with experiment.[3] Therefore, we suggest that, due to the possibility of these defects being formed, the decreased value of the measured spin polarizations—with respect to their bulk value—could be ascribed to this kind of defect, in addition to surface effects or other more complicated defects.

In order to investigate the spatial localization of the defect-induced gap states, we show in the inset of Fig. 3 the DOS at E_F for the minority component; this is expected to decay as we move away from the defect. Indeed, we find that the peak in the DOS is mainly confined in the region around the defective site. Even though some small deviations from the bulk also occur away from the defect, the main defect-induced changes are quite efficiently screened out. Therefore, we infer that the gap states are localized both spatially—as shown by the decay of DOS at E_F in the inset of Fig. 3—and energetically—as shown by the <0.1 eV energy spreading of the defect induced peak.

Further insights about the spatial localization of the defect–induced changes can be gained from an analysis of

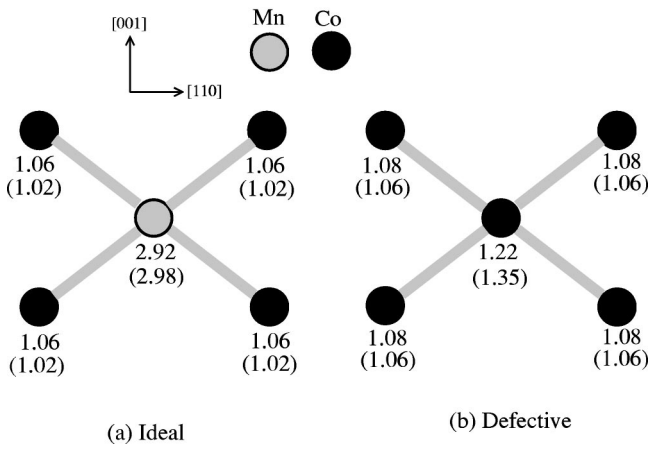

FIG. 4. Magnetic moments within MT spheres for (a) ideal and (b) defective systems for the Co antisite in Co_2MnSi around the defect. Values in parenthesis denote magnetic moments for equivalent atoms in Co_2MnGe.

the magnetic moments of the Co defect and of their Co first-nearest-neighbors (shown in Fig. 4). As in the previous Mn-antisite case, most of the variation of the total magnetic moment with respect to the ideal value is due to the defect atomic site, whereas already the first-nearest-neighbor shell largely recovers the magnetic moment typical of the bulk. This confirms the localized nature of the defect-induced changes.

C. Co-Mn swaps in Co_2MnSi

Let us now focus on atomic interchanges and consider Mn-Co swaps; this defect can also be viewed as the sum of two different Mn and Co atomic antisites that tend to aggregate. This defect shows a pretty high formation energy; however, this is of the same order of magnitude as the sum of the separated defects (Mn and Co antisites)—which might indicate that point defects have more or less the same probability to cluster, leading to this kind of disorder, or to remain isolated.

The calculated integer total magnetic moment suggests a half-metallic behavior. Indeed, this is shown by the total DOS (see Fig. 5). A comparison with the ideal situation shows that the majority DOS is basically unaffected; on the other hand, the occupied minority DOS shows a small shift (about 0.1–0.2 eV) towards higher binding energies, along with a defect-induced peak located at -0.2 eV below E_F. Therefore, due to its energy position, this peak is not as crucial as in the Co-antisite case and half metallicity is kept by Co-Mn swaps. Moreover, our results are in overall agreement with those reported by Orgassa *et al.*[9] for NiMnSb: in the case of $Ni_{1-x}Mn_xSb$ disorder—similar to the Mn-Co swap considered here—a peak just below E_F arises in the minority-spin component of the total DOS. This peak broadens in energy as the percentage of defects is increased, finally reaching E_F and resulting in the loss of half metallicity (see Fig. 1 of Ref. 9). In our case, we have a very similar behavior, except for the more ''energetically localized'' nature of the peak; we think that this quantitative disagreement

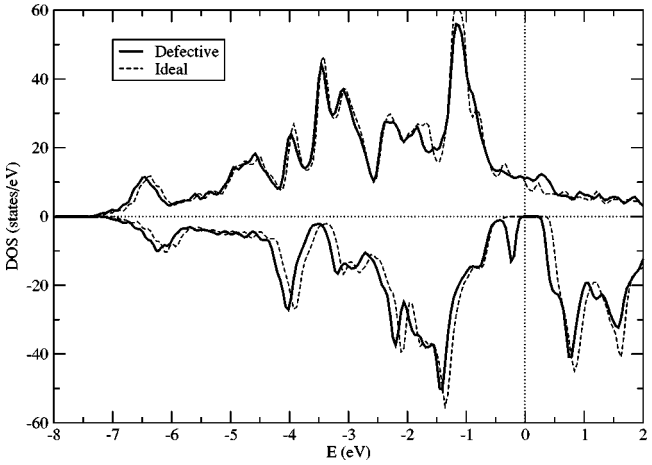

FIG. 5. Total DOS for defective (solid bold line) and ideal (dashed line) Co_2MnSi with Co-Mn swap in Co_2MnSi.

might be due to the computational method—layer Korringa-Kohn-Rosoker in conjunction with the coherent potential approximation—used in Ref. 9.

The magnetic moments (shown in Fig. 6) in the defective region show quite an interesting behavior: almost two Bohr magnetons are given up by the Co substituting for Mn and another two Bohr magnetons are given up by the Mn substituting for Co. As a result, the total magnetic moment is reduced by $4\mu_B$ (i.e., the difference between the bulk and defective total magnetic moments, $40\mu_B$ and $36\mu_B$, respectively). It is also interesting to note that the swaps induce a behavior similar to that of the single point defects; in fact, in this case, the magnetic moment for Mn substituting for Co is $-0.83\mu_B$, to be compared with $-0.87\mu_B$ for the Mn antisite. Similarly, the magnetic moment for Co substituting for Mn is $1.05\mu_B$, to be compared with $1.22\mu_B$ for the Co antisite. This shows that the first coordination shell (similar[17] in the case of isolated point defects and for the swaps) mainly dictates the behavior of the magnetic moments.

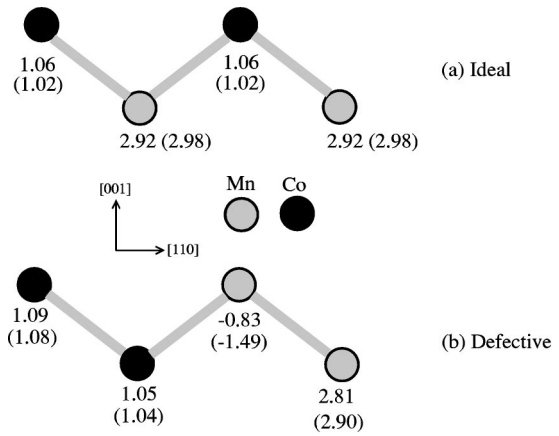

FIG. 6. Magnetic moments within MT spheres for (a) ideal and (b) defective systems for the Co-Mn swap in Co_2MnSi around the defect. Values in parenthesis denote magnetic moments for equivalent atoms in Co_2MnGe.

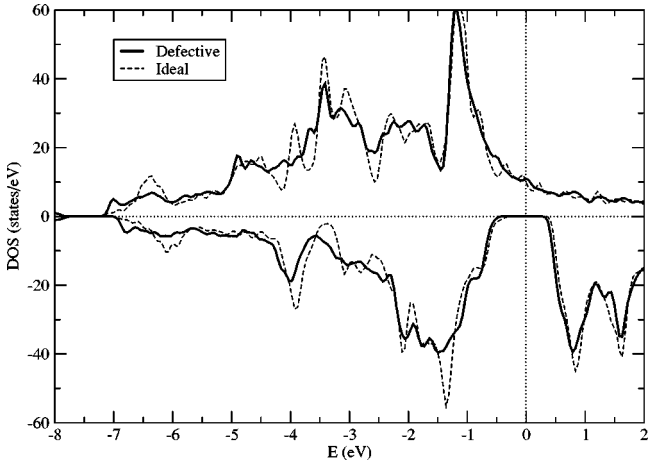

FIG. 7. Total DOS for defective (solid bold line) and ideal (dashed line) Co_2MnSi with Mn-Si swap in Co_2MnSi.

D. Mn-Si swap in Co_2MnSi

As shown by Table I, the highest formation energy among the cases studied is shown by the Mn-Si swap; therefore, the occurrence of an appreciable concentration of this kind of defect can definitely be ruled out. This is consistent with experiments which show that the Si site is fully occupied by Si, indicating that any disorder in Co_2MnSi does not involve Si. On the other hand, our findings are at variance with other first-principles predictions for the NiMnSb half-Heusler alloy: according to Orgassa *et al.*[9], the Mn-Sb (analogous to the Mn-Si here considered) disorder seems likely.

As far as the electronic and magnetic properties are concerned, a comparison between the total DOS (see Fig. 7) in the ideal and defective cells shows only minor defect-induced changes. In particular, in the energy region around E_F, the DOS is very similar for both minority- and majority-spin components, resulting in the same band-gap and half-metallic character as for the pure bulk. As a result, the Mn-Si swap system shows a total magnetic moment equal to that of the ideal Heusler alloy. This is consistent with the atomic magnetic moments shown in Fig. 8: within $0.04\ \mu_B$, the defect only results in a swap between the

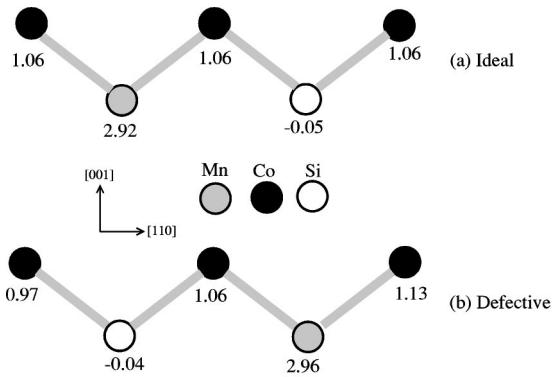

FIG. 8. Magnetic moments within MT spheres for (a) ideal and (b) defective systems for the Mn-Si swap in Co_2MnSi around the defect.

Mn and Si magnetic moments. Again, this shows that the first coordination shell—which in this case is exactly the same as the one in the bulk for both the exchanged atoms—is the most relevant in the formation of the bonds, local charge and spin-density rearrangement, and resulting magnetic moments.

E. Comparison between Co_2MnSi and Co_2MnGe

As already pointed out, we previously showed in Ref. 10 in the case of Co antisites in Co_2MnGe that gap states can result in the loss of half metallicity due to defect-induced states that arise in proximity to the Fermi level. This is similar to our present findings for Co_2MnSi; in fact, both the spatial behavior and energy behavior of defect-induced gap states suggests that Co antisites show a similar behavior in Co_2MnGe and Co_2MnSi. We remark that in the Co-antisite case, the loss of half metallicity in Co_2MnGe is also shown by the noninteger total magnetic moment (see Table I), whereas for the Si-based compounds the total moment is still close to an integer value and the loss of half metallicity is evidenced by the analysis of the total DOS. Moreover, we also calculated the defect concentrations for Co_2MnGe considering two different growth temperatures: $T_1 = 825$ K as reported in Ref. 4 for films via pulsed laser deposition and $T_2 = 165$ K, as reported in Ref. 10 for films grown via molecular-beam epitaxy (MBE). As expected, the two different temperatures result in very different concentrations: in the case of the MBE growth, all the defects have an almost negligible probability of being formed, whereas in the higher-temperature growth, the concentration of Mn atoms occupying the Co site is of the order of $<1\%$ and other defects have much smaller densities.

In order to compare the behavior of the defects considered in Co_2MnSi and Co_2MnGe, we report in parenthesis in Figs. 2, 4, and 6 the value of the atomic magnetic moments in the region around the defect site. The two different hosts globally show a very similar behavior in terms of magnetic moments, suggesting that the larger lattice constant or the smaller minority band gap of the Ge-based compound are not really relevant in the final determination of the magnetic properties. Quantitatively, the most sensible differences are shown by the Co-antisite case: there is about a $0.4\mu_B$ difference between the total magnetic moments in Co_2MnSi and Co_2MnGe (see Table I). Figure 4 shows that this difference is almost entirely due to differences in the central Co antisite, which changes from about $-0.9\mu_B$ in Co_2MnSi to about $-1.4\mu_B$ in Co_2MnGe, due to a very small difference in the energy position (<0.05 eV) of the defect-induced peak with respect to E_F.

Finally, it is interesting to note that the position of the defect-induced peak in the DOS with respect to E_F—and the related energy position of the conduction-band minimum in the minority-spin component—is very similar: for both Co_2MnSi and Co_2MnGe, the peak is basically coincident with E_F in the case of the Co antisite, whereas it lies at about -0.2 eV in the case of the Co-Mn swap. Except for very small differences that can be traced back to differences in the ideal bulk hosts (see Ref. 2 for details), the calculated DOS for antisite and swap defects in Co_2MnGe are not shown, due to very similar behavior to Co_2MnSi.

IV. CONCLUSIONS

In summary, by means of *ab initio* FLAPW calculations performed for different defects in Co_2MnSi and Co_2MnGe, we were able to show that both Co and Mn antisites, due to low formation energies, are likely to be formed in a concentration as high as 8%; on the other hand, atomic swaps (such as Co-Mn and Mn-Si swaps) have lower defect densities. Moreover, half metallicity, typical of the ideal Heusler alloy, is preserved in all cases, except for the Co antisite, where a defect-induced peak arises at the Fermi level. Our findings suggest that the loss of half metallicity found in experiments could be due to the presence of Co antisites, since the *s* component of the spin polarization at E_F in Co_2MnSi is in excellent agreement with tunneling measurements.

ACKNOWLEDGMENTS

We gratefully acknowledge support from INFM through Iniziativa Trasversale Calcolo Parallelo.

[1] S. Fujii, S. Sugimura, S. Ishida, and S. Asano, J. Phys.: Condens. Matter **2**, 8583 (1990).
[2] S. Picozzi, A. Continenza, and A.J. Freeman, Phys. Rev. B **66**, 094421 (2002).
[3] M. Raphael, B. Ravel, M. Willard, S. Cheng, B. Das, R. Stroud, K. Bussmann, J. Claassen, and V. Harris, Appl. Phys. Lett. **79**, 4396 (2001).
[4] B. Ravel, J.O. Cross, M.P. Raphael, V.G. Harris, R. Ramesh, and V. Saraf, Appl. Phys. Lett. **81**, 2812 (2002).
[5] M.P. Raphael, B. Ravel, Q. Huang, M.A. Willard, S.F. Cheng, B.N. Das, R.M. Stroud, K.M. Bussmann, J.H. Claassen, and V.G. Harris, Phys. Rev. B **66**, 104429 (2002).
[6] T. Ambrose, J.J. Krebs, and G.A. Prinz, J. Appl. Phys. **87**, 5463 (2000).
[7] B. Ravel, M.P. Raphael, V.G. Harris, and Q. Huang, Phys. Rev. B **65**, 184431 (2002).
[8] S. Ishida, T. Masaki, S. Fujii, and S. Asano, Physica B **245**, 1 (1998).
[9] D. Orgassa, H. Fujiwara, T.C. Schulthess, and W.H. Butler, Phys. Rev. B **60**, 13 237 (1999); J. Appl. Phys. **87**, 5870 (2000).
[10] S. Picozzi, A. Continenza, and A.J. Freeman, J. Appl. Phys. **94**, 4723 (2003).
[11] J.P. Perdew, K. Burke, and M. Ernzernhof, Phys. Rev. Lett. **77**, 3865 (1996).
[12] E. Wimmer, H. Krakauer, M. Weinert, and A.J. Freeman, Phys. Rev. B **24**, 864 (1981).

[13] H.J. Monkhorst and J.D. Pack, Phys. Rev. B **13**, 5188 (1976).
[14] S.B. Zhang *et al.*, Phys. Rev. B **57**, 9642 (1998).
[15] T. Asada and K. Terakura, Phys. Rev. B **47**, 15 992 (1993), and references therein.
[16] C.G. Van de Walle *et al.*, Phys. Rev. B **47**, 9425 (1993).
[17] In the isolated point case: (i) when Co substitutes for Mn, the first coordination shell of the defect is made of eight Co atoms; (ii) in the Mn antisite case, the first coordination shell of the defect is made of four Mn and four Si atoms. On the other hand, in the Co-Mn swap, the exchanged Mn has the first coordination shell made of three Mn, one Co and four Si atoms, whereas the exchanged Co has the first coordination shell made of seven Co and one Mn atoms.